CHAPTER

DIELECTRIC PROPERTIES OF $Y_{1/3}La_{1/3}Cu_3Ti_4O_{12}$ SYNTHESIZED BY SEMI-WET ROUTE

4

4.1 INTRODUCTION

The multifunctional materials are the demands of future nanotechnology. It is highly desirable to integrate multi-functionality in a single material to fulfill the criteria of device miniaturization and high-density data storage in the same system. The perovskite materials provide a building block for new bottom-up approaches due to their intrinsic size-dependent properties and resulting applications. In recent years, studies of newer type of nano-sized dielectric materials and their isomorphs has been of keen interest. The requirement of new, innovative and easily obtainable dielectric materials that produces high dielectric permittivity with a very low dielectric loss (tan δ) has always received considerable attention (Hongtao *et al.*, 2000). The $CaCu_3Ti_4O_{12}$ (CCTO) complex perovskite has attracted much interest due to its high dielectric constant (10^4-10^5) which is almost frequency independent (10^2-10^6 Hz) and shows excellent thermal stability in the temperature range, 100-600 K (Subramanian *et al.*, 2000; Ramirez *et al.*, 2000). A big problem in using this material for miniaturization of electronic devices is its high dielectric loss. The complex perovskite structure of CCTO is highly flexible. Its dielectric constant and dielectric loss depends significantly on the various cationic substitutions such as La at Ca and Zn, Mn, Mg at Cu and Cr, Hf at Ti site (Li *et al.*, 2006; Feng *et al.*, 2006; Ni *et al.*, 2009; Rai *et al.*, 2009; Hutagalung *et al.*, 2009; Li *et al.*, 2010; Xu *et al.*, 2011; Zheng *et al.*, 2012). It also depends on the synthesis routes (Hassini *et al.*, 2001; Jin *et al.*, 2007) as well as the processing conditions, such as sintering temperature (Aoyagi *et al.*, 2007; Prakash *et al.*, 2006), sintering time (Kaur *et al.*, 2010), cooling rate and partial pressure of sintering atmosphere (Thongbai *et al.*, 2007).

Various isostructural materials based on complex perovskite structure, like $ACu_3Ti_4O_{12}$ (A = $Y_{2/3}$, $Bi_{2/3}$, $La_{2/3}$, $Nd_{2/3}$, $Sm_{2/3}$, $Gd_{2/3}$, $Dy_{2/3}$) also exhibit similar

dielectric properties with good thermal stability (Liu *et al.*, 2005). Apart from this, a broad range of doping or partial substitution may be carried out at A, Cu or Ti-site of $ACu_3Ti_4O_{12}$. It is quite inspiring to investigate systematically new $ACu_3Ti_4O_{12}$ like materials possessing temperature independent high dielectric constant and low dielectric loss with excellent thermal stability. Such high dielectric constant materials need a wide frequency range from an application point of view; especially over 1 MHz. Rare earth doping can be applicable in significant improvement in the working frequency band. Very few works have been reported on $Y_{2/3}Cu_3Ti_4O_{12}$ (YCTO) material (Liang *et al.*, 2012; Li *et al.*, 2015). It has almost the same crystal structure to that of CCTO. Doping of $Y_{2/3}Cu_3Ti_4O_{12}$ at different sites may disclose much information about microstructure and other properties related to it. It may also enhance the properties related to dielectric constant. The partial isovalent substitution of several cations with comparable ionic radii at different interstices can improve properties associated with ferroelectricity and dielectric response in this material. It is expected that structural flexibility and chemical versatility of YCTO materials could make them more suitable for device applications.

In this chapter, we have synthesized $Y_{1/3}La_{1/3}Cu_3Ti_4O_{12}$ (YLCTO) ceramic by the semi-wet route. In this ceramic, Y^{3+}-site was doped by La^{3+} in pure $Y_{2/3}Cu_3Ti_4O_{12}$ (YCTO) ceramic. Further, the phase structure, microstructure and dielectric properties of this rare earth based materials are analyzed with the help of TG/DTA, XRD, SEM, EDX, AFM and TEM techniques. The dielectric property has been studied in a wide range of frequency 2Hz - 5MHz at different temperature 35-227 $^{\circ}$C.

4.2 RESULTS AND DISCUSSION

4.2.1 Thermal Analysis

Fig. 4.1 illustrates the simultaneous TG/DTA/DTG plots of precursor dry powder of YLCTO in the same thermal conditions as discussed in the section 3.2.1. TG clearly shows three stages of weight loss with increasing temperature up to 950 $^{\circ}$C. The first significant weight loss occurred at 280 $^{\circ}$C, second at 860 $^{\circ}$C and the third one with very small weight loss around 970 $^{\circ}$C. The corresponding DTG curve shows one strong exothermic peaks near 835 $^{\circ}$C besides a small peak around and 963 $^{\circ}$C. It is

also observed that DTG peaks are more intense than DTA peaks. It is expected that the final product formed around 963 °C.

The first weight loss around 280 °C is due to an exothermic reaction which may be attributed to the elimination of residual water and dehydration of the hydrated gel. The second weight loss observed at 860 °C is due to the formation of an intermediate complex which is further supported by the presence of exothermic peak observed at 835 °C in the DTA curve. The third weight loss around 970 °C is due to an exothermic addition reaction of an intermediate compound with TiO_2 to give the final product $Y_{1/3}La_{1/3}Cu_3Ti_4O_{12}$. We can conclude that the ideal sintering temperature for the formation of single phase of precursor dry powder of YLCTO is 970 °C.

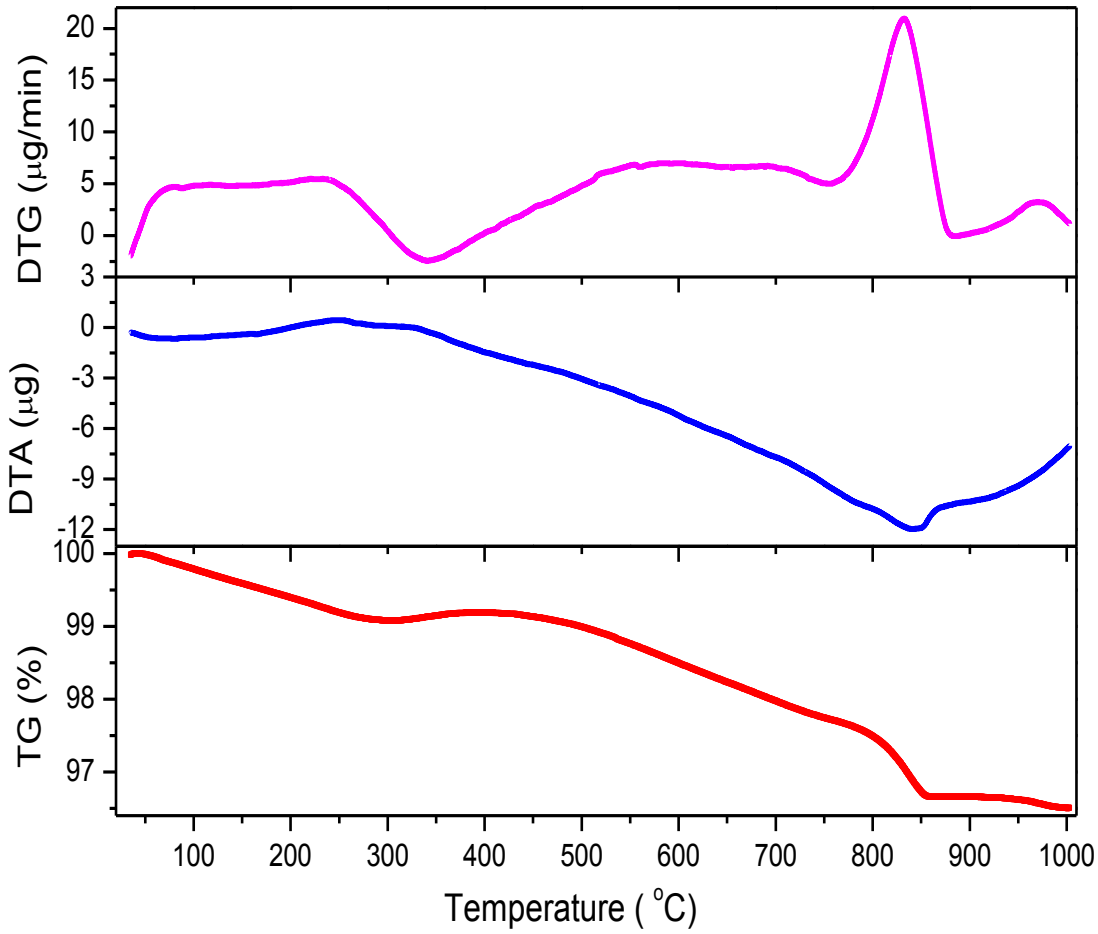

Figure 4.1: DTA/TGA curves for $Y_{1/3}La_{1/3}Cu_3Ti_4O_{12}$ (YLCTO) precursor powder.

4.2.2 X-Ray Diffraction Analysis

XRD pattern of YLCTO ceramic sintered at 950 °C for 12 h is shown in Fig. 4.2. It clearly shows YCTO phase along with the presence of minor secondary phase of CuO (JCPDS card no. 80-1917). The main XRD diffraction peaks of YLCTO corresponding to (220), (310), (222), (321), (400), (422), (440) planes were found to have a good matching to those of $CaCu_3Ti_4O_{12}$ (JCPDS 75-2188). In contrast to undoped YCTO, Lanthanum doped YCTO ceramic shows absence of XRD diffraction peak (at $2\theta = 27.43$) corresponding to (211). The XRD data were indexed on the basis of a cubic unit cell similar to CCTO. The lattice parameter and unit cell volume of YLCTO ceramic were determined by least square refinement method using 'CEL' software. The value of lattice parameter and unit cell volume was found to be 7.4016Å and 405.4894(Å)^3 respectively. XRD pattern shows the presence of split peaks for the reflections 400, 422 and 440. This may be due to the presence of Cu-$K\alpha_2$ along with Cu-$K\alpha_1$ in the X-ray radiations used for diffraction which is supported by the fact that in all these reflections, the intensity of peaks due to Cu-$K\alpha_2$ is close to 50% of the intensity of peak due to Cu $K\alpha_1$ as expected (Culity *et al.*, 2001).

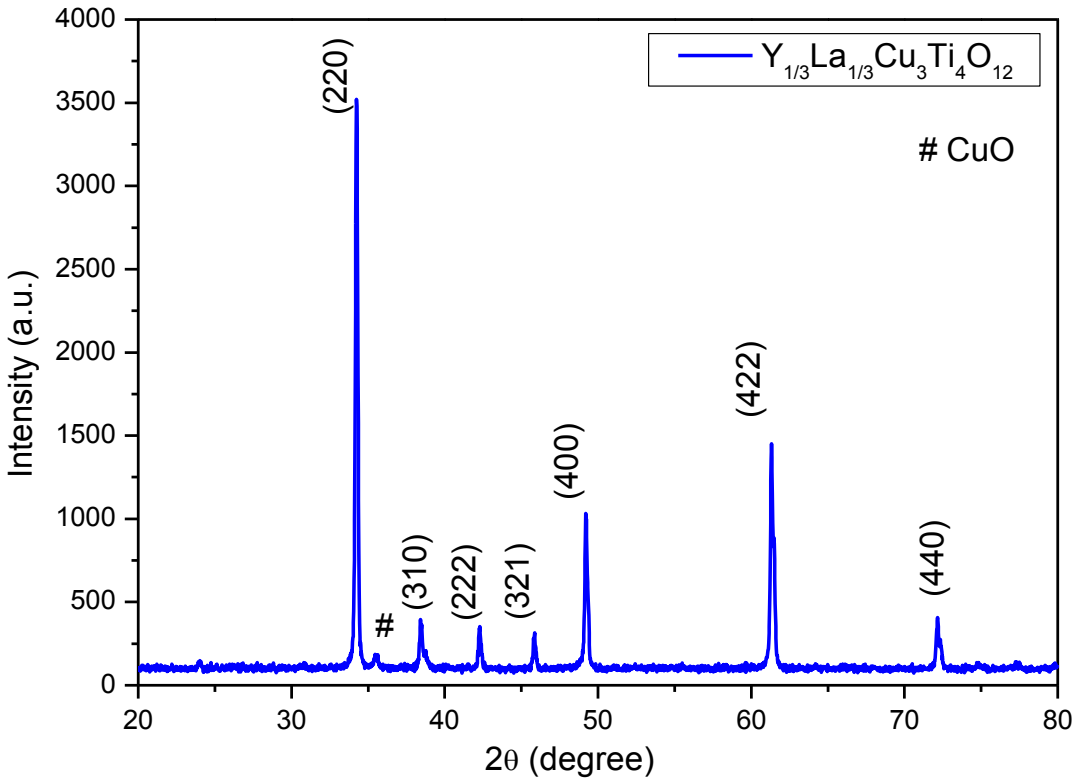

Figure 4.2: XRD patterns of YLCTO ceramic sintered at 950 °C for 12h.

The crystallite size (D) of the YLCTO ceramic was determined using the Debye-Scherrer's formula as given below:

$$D = \frac{k\lambda}{\beta \cos\theta} \qquad (4.1)$$

where k is the crystal shape coefficient (k = 0.89), λ is the wave length, β is the corrected full width at half maximum (FWHM) which was obtained by correction of the peak broadening due to instrument and θ is diffraction angle. The calculated value of crystallite size for the YLCTO ceramic was found to be 59 ± 2 nm and also listed in Table 4.1.

Table 4.1: Crystal structure, lattice parameter and unit cell volume of the undoped YCTO and La doped YCTO ceramic.

System	Structure	Lattice Parameter (Å)	Unit Cell Volume $(Å)^3$	Crystallite Size (nm) by XRD	by TEM
$Y_{2/3}Cu_3Ti_4O_{12}$	Cubic	7.4983	421.5833	68 ± 6	60 ± 20
$Y_{1/3}La_{1/3}Cu_3Ti_4O_{12}$	Cubic	7.4016	405.4894	59 ± 5	46 ± 8

4.2.3 Scanning Electron Microscopic and Energy Dispersive X-ray Spectroscopic Studies

Fig. 4.3 exhibits the scanning electron micrograph of the fractured surface of YLCTO ceramic sintered at 950 °C for 12h. The SEM micrograph clearly displays smooth surfaced grains having a bimodal structure with some pores. The microstructure is dominated by small spherical grains of size 1-2 μm. However, few cubical grains of size below 1.2 μm are also present. It is also observed that there is no distinct grain boundary present. The absence of grain boundary may be due to lower sintering temperature. The secondary phases were also not observed in SEM micrographs. Such similar structure is analogous to the result obtained for CCTO ceramics sintered at low temperatures (Shao *et al.*, 2006; Pan *et al.*, 2005).

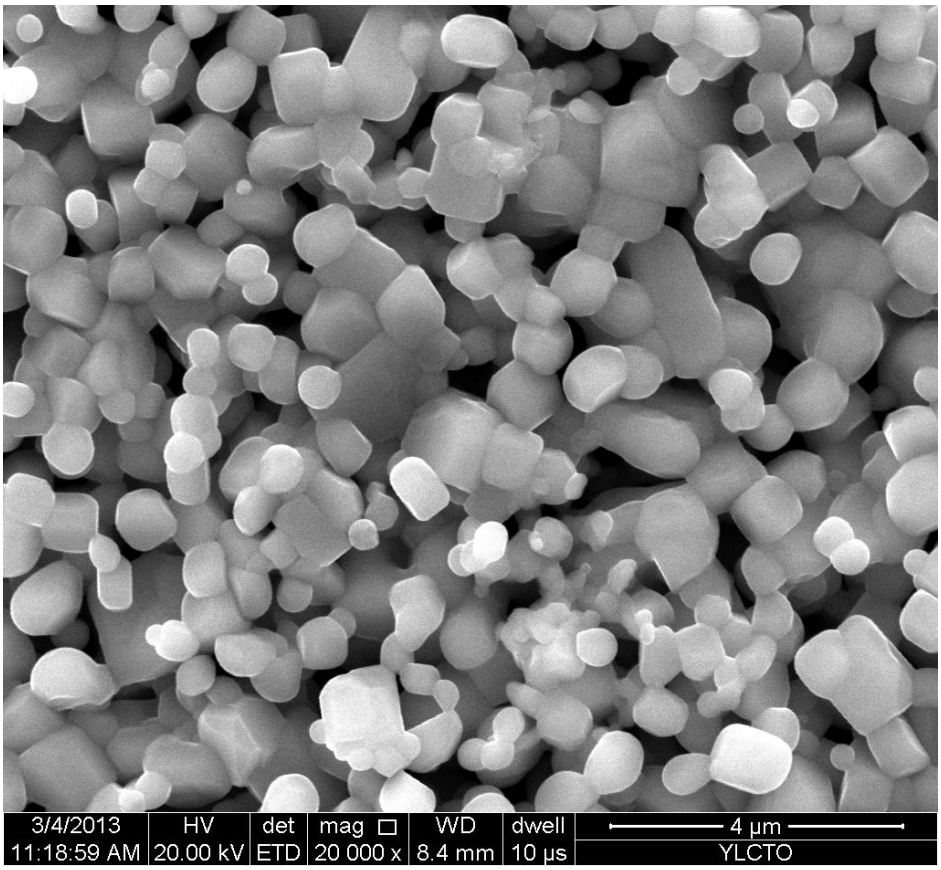

Figure 4.3: SEM micrographs of sintered $Y_{1/3}La_{1/3}Cu_3Ti_4O_{12}$ (YLCTO) ceramic.

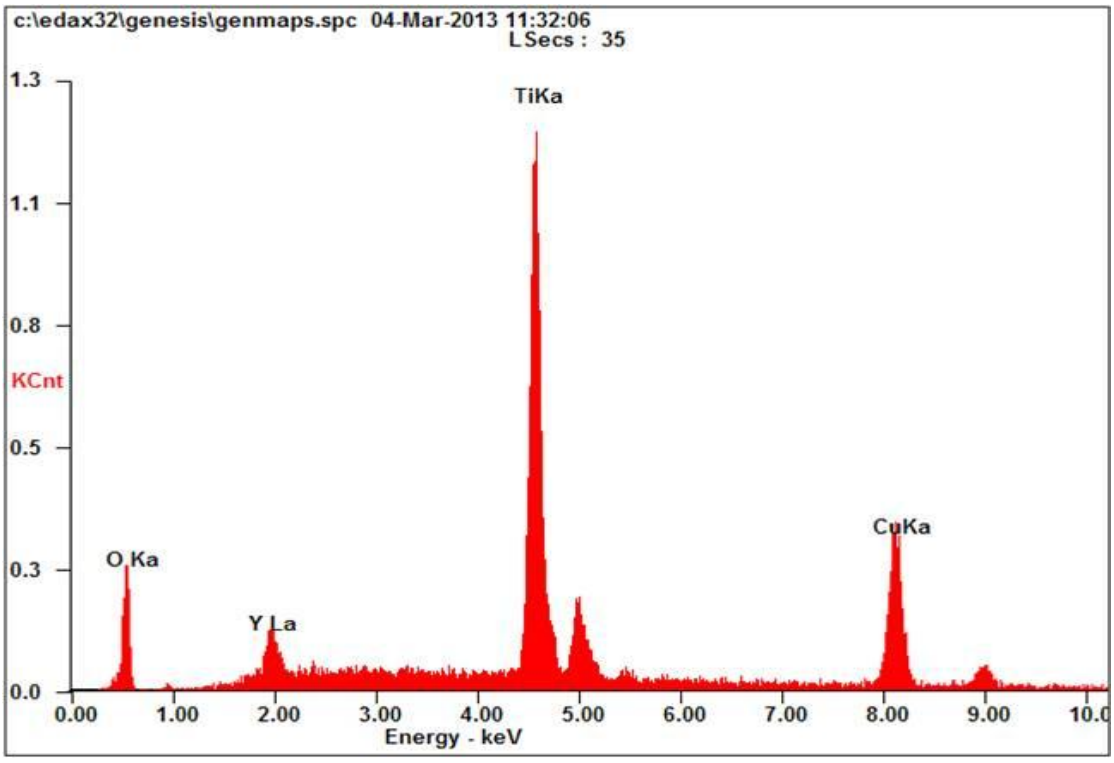

Figure 4.4: EDX spectra of $Y_{1/3}La_{1/3}Cu_3Ti_4O_{12}$ (YLCTO) sintered at 950 ^oC for 12h.

More frequent, but large grain growth is caused due to the presence of liquid phase along the grain boundaries. The amount of CuO phase along the grain boundaries may contribute significant effects to promote the grain growth and densification. It is also established that increase in sintering temperature significantly promotes the grain growth and microstructural densification. It is also evident from Fig. 4.3 that YLCTO ceramic shows high degree of porosity. The calculated value of porosity in YLCTO ceramic was found to be 6.3%. The high porosity may be attributed to the formation of oxygen vacancies during sintering. It may also be due to lower sintering temperature. An increase in the sintering temperature may lead to a decrease in porosity owing to the grain growth phenomena. The calculated value of the density of YLCTO ceramic was found to be 5.94 g/cm^3 which is very close to the reported value of undoped YCTO ceramic (Liang *et al.*, 2012).

Fig. 4.4 shows EDX spectra of YLCTO ceramic indicating the presence of Y, La, Cu, Ti and O elements. Their atomic percentage was found to be 2.12, 0.87, 26.62 and 39.56 respectively. Quantitative data for atomic and weight percentage of the elements present in a grain of YLCTO ceramic obtained from EDX data were as per expected stoichiometry. It confirms the purity of YLCTO ceramic.

4.2.4 Atomic Force Microscopic Study

The surface topography of $Y_{1/3}La_{1/3}Cu_3Ti_4O_{12}$ (YLCTO) ceramic was studied with the help of Atomic Force Microscopy. These images were obtained by a thin film deposition on amorphous glass substrate in a tapping mode. Fig. 4.5(a) depicts the two-dimensional AFM micrograph of YLCTO thin film which is smooth and compact. The small grains are scatted on its whole surface. The average grain size and average diameter of grain estimated to be 41.8 nm (Fig. 4.6a) and 47.1 nm (Fig. 4.6b) while the grains were homogeneously mounted over the substrate of an area 0.00204 μm^2 (Fig. 4.6c). The 2-Dimensional and 3-Dimensional surface roughness of a sample is investigated by amplitude and height analysis parameters, respectively. The amplitude analysis parameters mainly includes average roughness, root mean square roughness, maximum peak to valley height roughness, ten-point mean height roughness, skewness roughness and kurtosis roughness. Through the roughness parameters, the surface condition of the entire measured length or area will be evaluated in terms of peak and valley (Raposos *et al.*, 2007).

Based upon the statistical study of total 252 grain ensembles within the length 3.532 μm and scanning area 5 μm × 5 μm for two-dimensional AFM image of surface of YLCTO thin film, the value of average roughness (R_a) and Root mean square roughness (R_q) was estimated to be 2.552 and 3.249 nm. The average roughness gives the deviation of the calculated mean height over the measured area while Root mean square roughness demonstrates the standard deviation of the surface height over the measured area. The Maximum peak to valley height roughness (R_t) which summarizes the total roughness of the measured area was found to be 16.563 nm whereas the Ten-points mean height roughness (R_z) shows the mean height difference between the average of the five highest peaks and the five lowest valleys in the evaluation surface was found to be 12.195 nm.

The functional parameters such as skewness (R_{Sk}) and kurtosis (R_{Ku}) moments are used to measure the asymmetry and the flatness of the thin film, respectively. The Skewness roughness (R_{sk}) is used to measure the profile symmetry of the mean line was found to be 0.552, while the kurtosis roughness (R_{ku}) is used to measure the surface sharpness which is in fact, the distribution of the spikes above and below the mean line was found to be 3.166 which is more than 3. It indicates that the 2D-AFM image has more peaks than valleys. Apart from average roughness, the lower positive values of skewness roughness (R_{sk}) imply for the smoothness of surface with predominant peaks while higher positive value for kurtosis roughness (R_{ku}) indicating that the surface of scanned area of YLCTO thin film is slightly bumpy in nature due to the appearance of low number of high peaks and low valleys on the surface. It is more evident from the 3D AFM-image (Fig. 4.5 C). As kurtosis value is more than three, such distribution curve has many high peaks and low valleys.

Fig. 4.5(b) shows the grains and grain boundary regions in YLCTO thin film. It exhibits compact structure with granular morphology, buffer layer, plates like grains and clear grain boundary. Fig. 4.5(c) exhibits its three-dimensional surface morphology exhibits several peaks corresponding to grain with compact structure. Based upon the statistical study of total 1.26×10^5 grains within the scanning area 5 μm × 5 μm and sampling and evaluation area 25.019 μm^2 for the three-dimensional AFM image of YLCTO thin film surface, the value of average roughness (Sa), Root mean square roughness (Sq), maximum peak to valley height roughness (S_z) and 10-

points mean height roughness (S_{10z}) was estimated to be 2.684, 3.945, 60.595 and 53.788 nm, while skewness (S_{ku}) and kurtosis (S_{sk}) was found to be 2.391 and 17.549. A high positive value of skewness indicates the asymmetric type of distribution. It also confirms that YLCTO surface has more peaks than valleys. The Kurtosis value is greater than 3, confirming the distribution curve to be Leptokurtoic which in turn, is characterized by many high peak but low valley. It is also agreement with the 3D AFM-image. 3D surface analysis refines the data and findings obtained in 2D mode in a more accurate way.

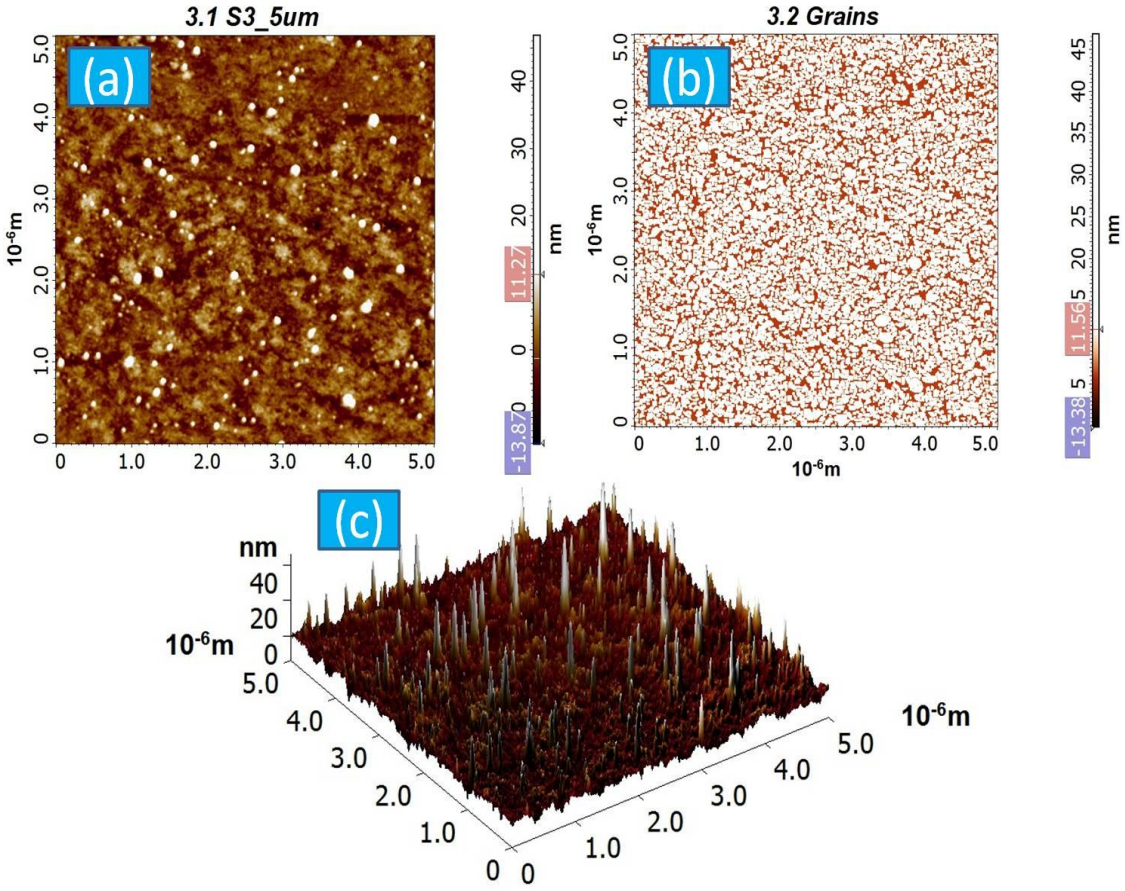

Figure 4.5: (a) 2- dimensional AFM micrograph of thin film of (b) 2-dimensional AFM micrograph showing grain boundary (c) 3- dimensional AFM micrograph of sintered $Y_{1/3}La_{1/3}Cu_3Ti_4O_{12}$ ceramic.

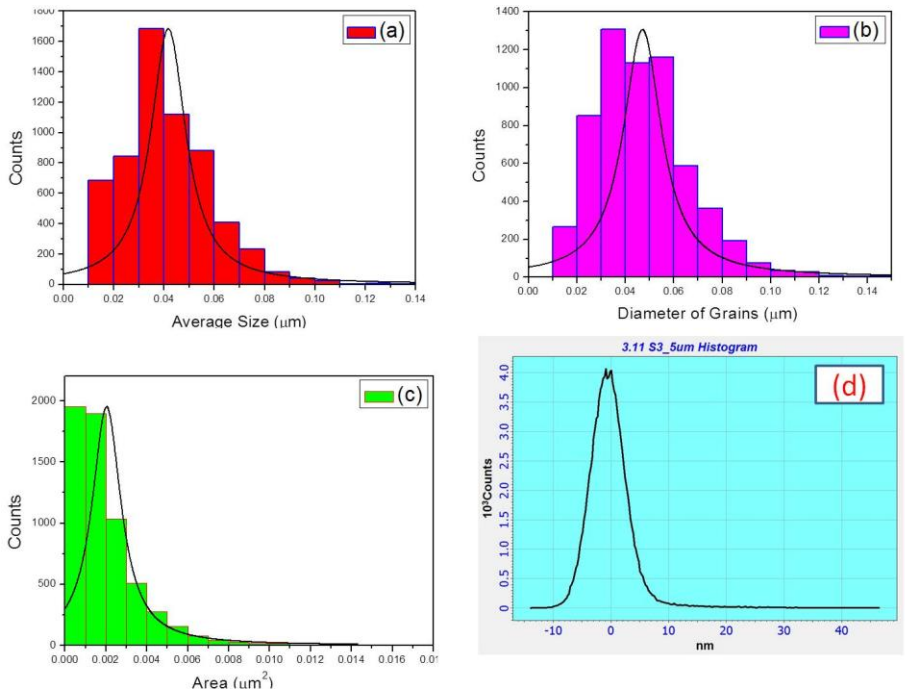

Figure 4.6: Different histograms for sintered $Y_{1/3}La_{1/3}Cu_3Ti_4O_{12}$ ceramic exhibiting (a) Average size (b) Diameter of grains (c) Area of grains and (d) Average 3- dimensional roughness.

The surface roughness parameters of the tested sample in 2D and 3D AFM study of YLCTO thin film, deduced with the help of NOVA software are summarized in Table 4.2.

Table 4.2: The surface roughness parameters of $Y_{1/3}La_{1/3}Cu_3Ti_4O_{12}$ thin film obtained by 2D- and 3D- AFM-image mapping.

Details of Roughness	**Parameters**	
	Amplitude (2D)	**Height (3D)**
Average /Arithmetic	2.552	2.684
Root Mean Square	3.249	3.945
Maximum peak to valley height roughness	16.563	60.595
Ten-points mean height roughness	12.195	53.788
Skewness	0.552	2.391
Kurtosis	3.166	17.549

4.2.5 Transmission Electron Microscopy

The bright field TEM image of YLCTO ceramic sintered at 950 ^{o}C for 12h is presented in Fig. 4.7. The particles of YLCTO ceramic show an average size of 46 ± 8 nm. From the inset picture, it is clear that La doped YCTO ceramic shows agglomeration. The size of nanoparticles is in agreement with XRD results.

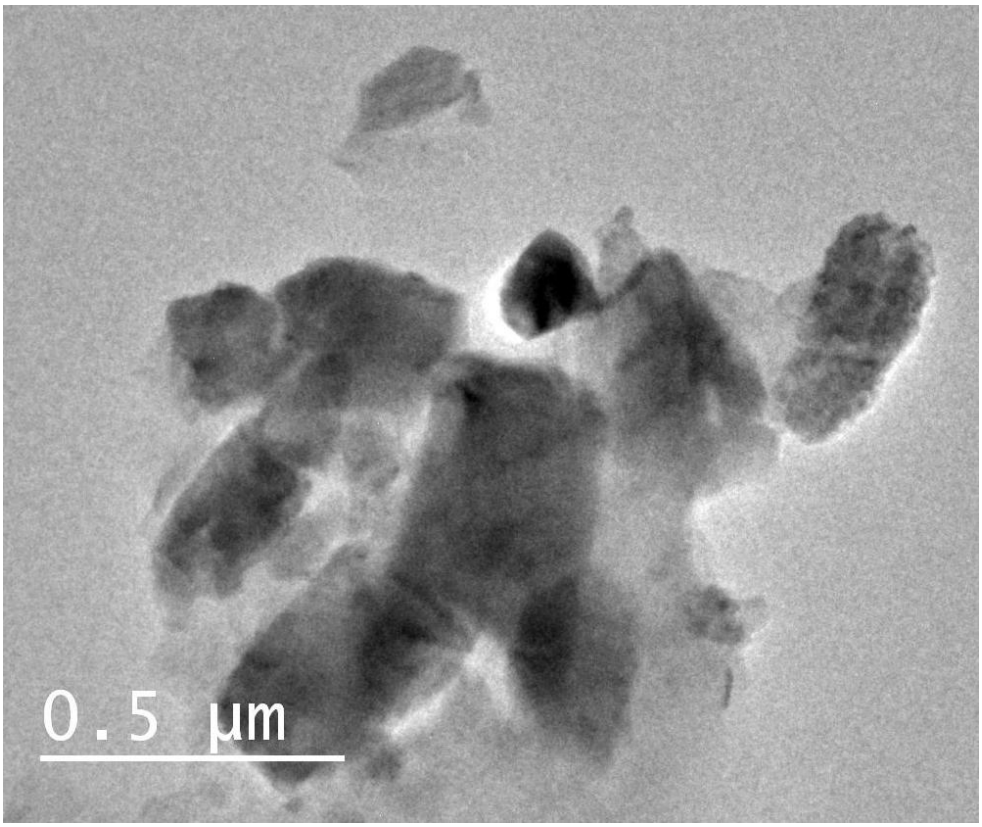

Figure 4.7: Bright Field TEM image of YLCTO ceramic sintered at 950 ^{o}C for 12h.

4.2.6 Dielectric and Electric Behavior

The plot of dielectric constant and tan δ of YLCTO ceramic at 0.1, 1, 10 and 100 kHz with variation of temperatures is shown in Fig. 4.8. The dielectric constant is nearly temperature independent from 300 K to 500 K at 10 and 100 kHz. At frequency 0.1 and 1 kHz), the dielectric constant is almost temperature independent from 300 K to 375 K and there after it increases with increasing temperature. It is also observed from the figure that the dielectric constant (ε′) for YLCTO samples was found to be 347, 260, 269 and 216 at 0.1, 1, 10 and 100 kHz respectively i.e. dielectric constant decreases with increasing frequencies. The dielectric constant (ε′) for YLCTO samples is lower than that of undoped YCTO ceramic.

It is also evident from the Fig. 4.8(b) that the value of tan δ remains constant from 308 K (RT) to 350K at 0.1, 1, 10 and 100 kHz respectively and after that, it increases with increasing temperature. The increase in the dielectric loss with increase in temperature may be due to increase in conductivity of YLCTO ceramic with temperature. The value of tan δ at room temperature for YLCTO ceramic was found to be 0.49, 0.16, 0.15 and 0.18 at 0.1, 1, 10 and 100 kHz, respectively. It is important to note that the dielectric loss decreases with increasing frequency for all compositions. The range of temperature independent behavior of dielectric loss gets increased slightly at 100 kHz. It is also significant that the value of dielectric loss for YLCTO is quite less than the undoped YCTO ceramic. Such an independent variation of both ε and tan δ from room temperature 300 to 350K is appreciable.

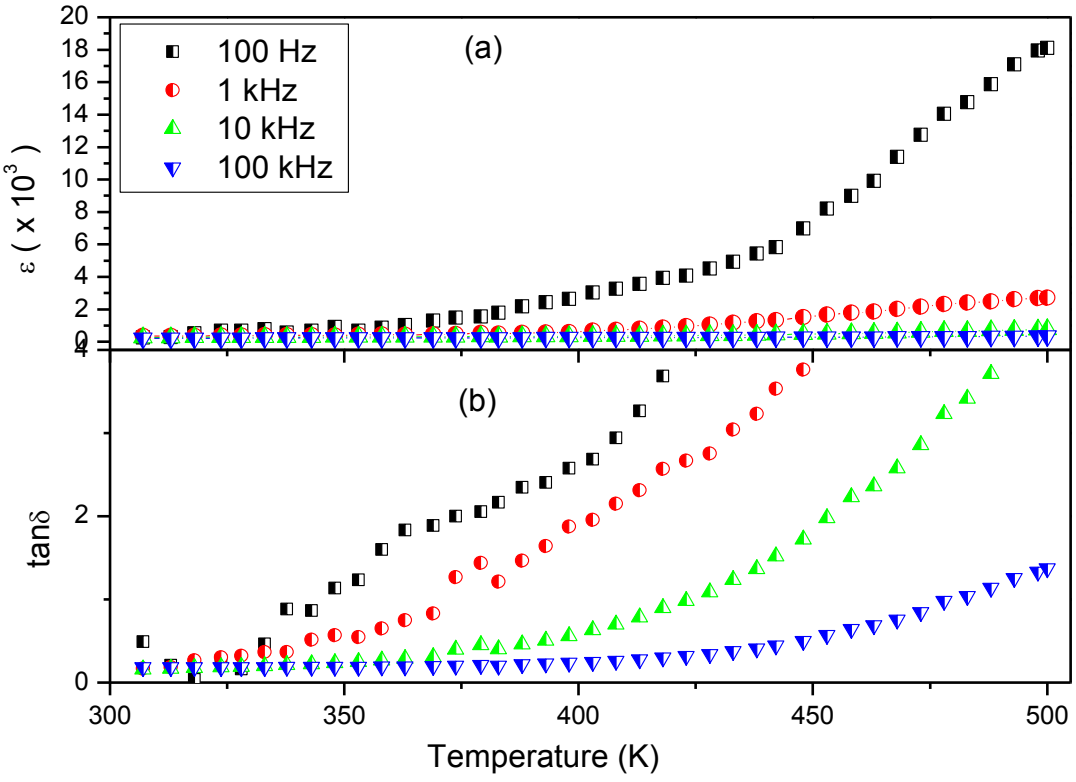

Figure 4.8: Variation of (a) bdielectric constant (ε′) and (b) tangent loss (tan δ) with temperature at a few selected frequency for sintered YLCTO ceramic.

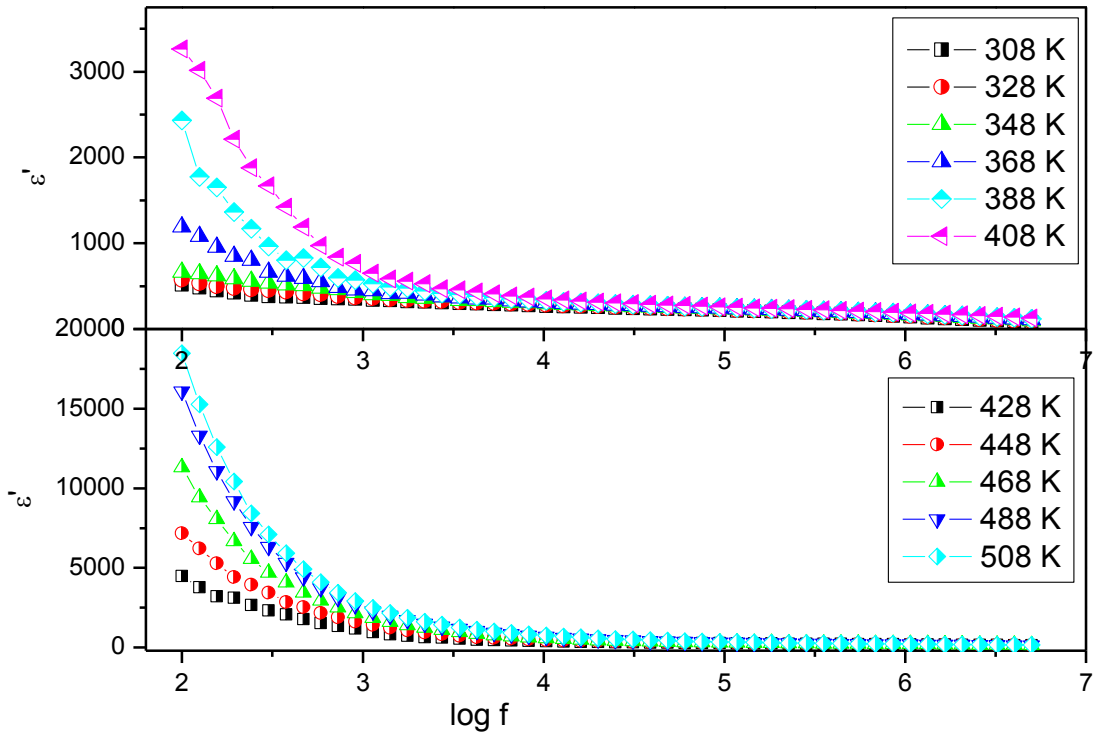

Figure 4.9: Plots of the real part of dielectric constant (ε′) with the variation of frequency at a few selected temperatures for sintered YLCTO ceramic.

The variation of dielectric constant (ε′) with frequency (10^2 - 10^6 Hz) at few selected temperature for YLCTO ceramic is shown in Fig. 4.9. The dielectric constant for YLCTO ceramic decreases rapidly in lower frequency ranges (10^2 Hz to 10^3Hz), then slowly in the frequency range (10^3 to 10^5Hz) and ultimately remains nearly constant between 10^5 Hz - 10^6 Hz. At lower frequencies, the dielectric constant values of YLCTO ceramic are high and the dielectric constant decreases with increasing frequency. The decrease in dielectric constant with frequency may be due to the contribution of space charge accumulation at the interface which leads to polarization of the ionic medium and hence increases the value of ε′. In high-frequency regions, the periodic reversal of the field takes place so rapidly that there is no charge accumulation at the interface, resulting in a constant ε′ value (Tareev 1975). However, the dielectric constant of YLCTO ceramic at a given frequency increases with increase in temperature. The value of ε′ for YLCTO ceramic was found to be 504 at 308 K and 100 Hz, which is much lower than the undoped YCTO ceramic (ε′ = 8434).

Dielectric absorption in a material is characterized by tan δ as well as ε'' values. Usually, a relaxation peak is obtained when ε'' and tan δ values are plotted against frequency. Such type of dielectric relaxation occurs when hopping frequency of charge carriers equals the frequency of applied field. But it is clear from the Fig. 4.10 that such relaxation peaks were absent in YLCTO ceramic at different temperature in the region of 100 Hz -5 MHz.

It is important to note that undoped YCTO ceramic gives the direct evidence for relaxor behavior with a characteristic dielectric relaxation peaks around 10^5–10^6 Hz frequency. The absence of relaxation peaks in YLCTO ceramic may be attributed to a reduction in the number of hopping as the concentration of Lanthanum increases. It is likely that the relaxation peaks corresponding to YLCTO ceramic may lie outside the measured frequency range.

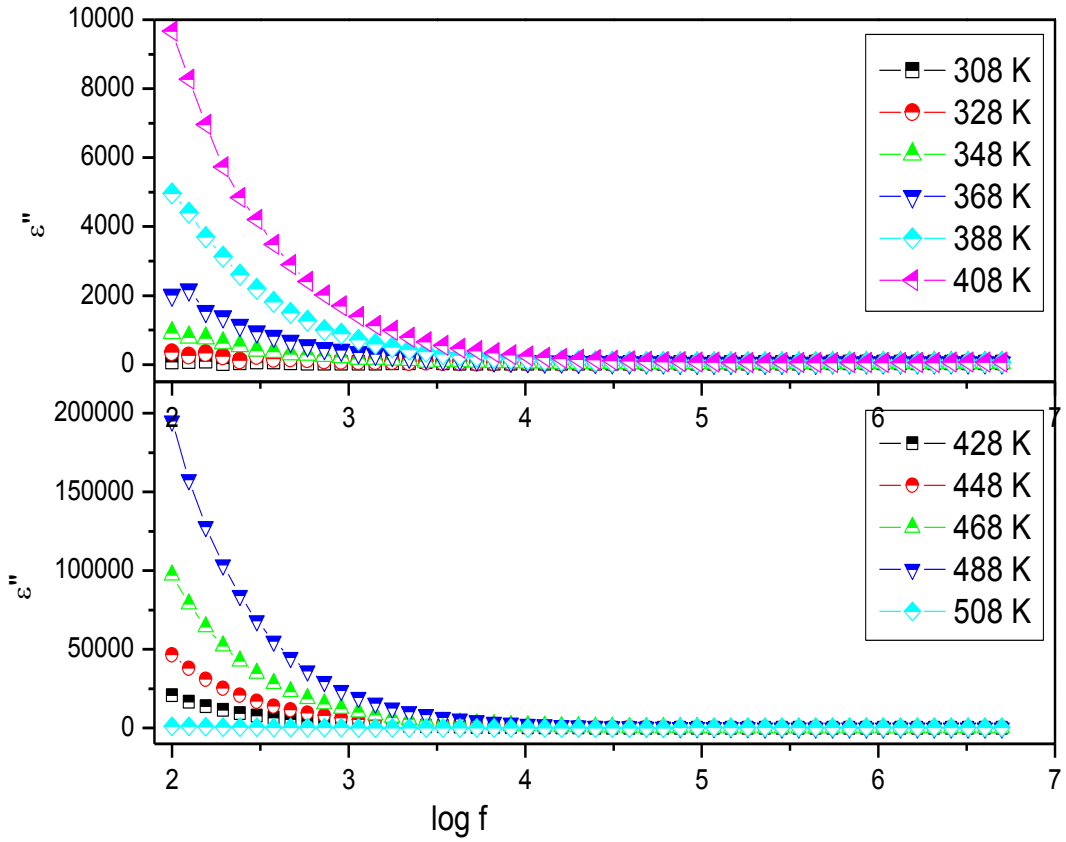

Figure 4.10: Variation of the imaginary part of dielectric constant (ε'') with frequency at a few selected temperatures for sintered YLCTO ceramic.

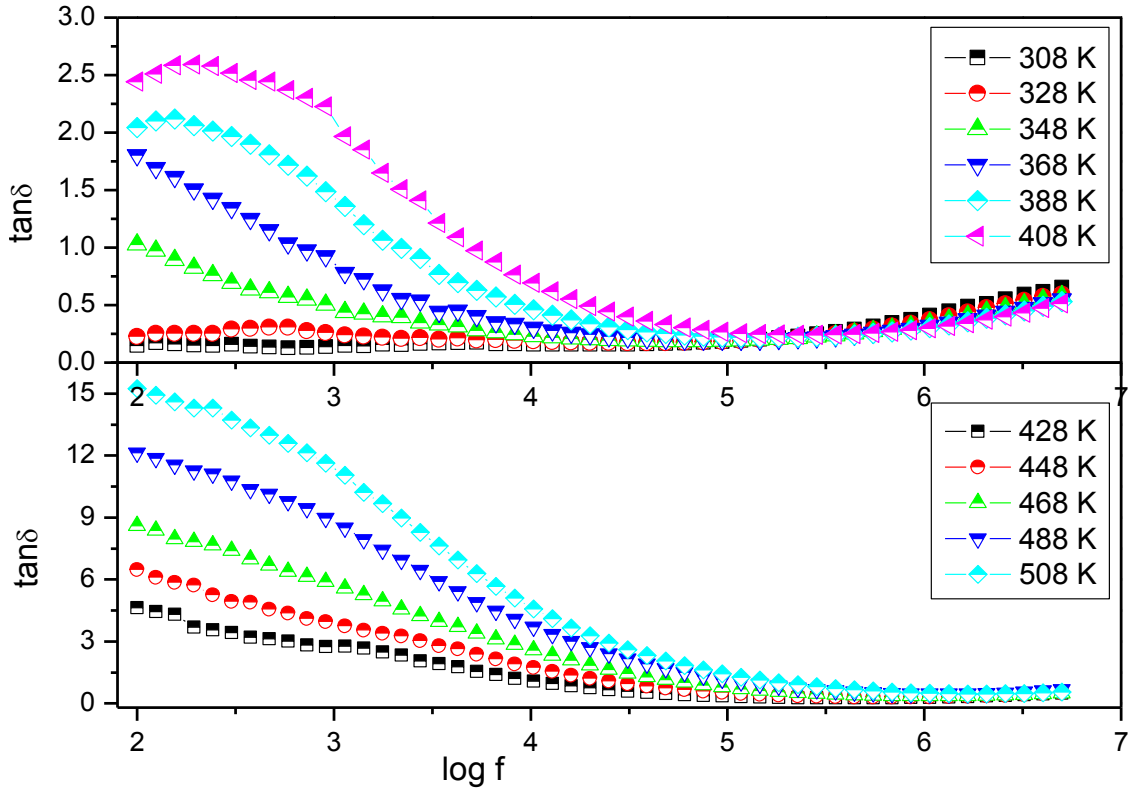

Figure 4.11: Variation of tangent loss (tan δ) with frequency at few selected temperature for sintered YLCTO ceramic.

Fig. 4.11 shows the variation of loss tangent (tan δ) with frequency at a few selected temperatures (308-500 K) and is characterized by the presence of relaxation peaks. These peaks shift to higher frequency regions with increase in temperature indicating the presence of Debye type Maxwell-Wagner relaxation. YLCTO ceramic shows the minimum dielectric loss (tan $\delta \sim 0.11$) at 308 K at 10 kHz. The dielectric loss of YLCTO ceramic was found to be 0.11 to 0.69 (308 to 408 K) and 1.05-4.03 (428- 500 K) at 10 kHz frequency. The dielectric loss in a low-frequency region may be attributed to the conduction of oxygen vacancies originated by mass diffusion during sintering process, but the slight increases in the value of tan δ with frequency may be due to increase in conductivity associated with the grain boundaries. The insulating nature of grain boundary may be attributed to the sintering effects and its doping conditions. Usually, oxygen diffusion takes place during the sintering due to the difference in the partial pressure of oxygen in the ceramic oxide and the atmosphere. As grain boundary is associated with a higher diffusion coefficient, the

rate of oxygen diffusion is usually more at grain boundary in comparison to grain and in turn, the extent of reoxidation is more at grain boundary during the process of cooling. These effects may lead to semiconducting grain and insulating grain boundary in YLCTO ceramic and support IBLC mechanism (Liu *et al.*, 2007).

4.2.7 Impedance spectroscopic studies

Electrical behavior of YLCTO ceramic has been characterized over a wide range of frequency and temperature. The complex impedance (Z*) plot was employed to ascertain the reasons for dielectric dispersion and formation of barrier layer in YLCTO ceramic. In polycrystalline materials, impedance formalism gives clear information about the grain boundary conduction effects while the bulk effect gets dominated by the electric modulus formalism.

The Nyquist plot between *Z*' and *Z*" of sintered YLCTO ceramic at a few selected temperature is shown in Fig. 4.12. It is clear from the graph that all the curves exhibit a common tendency to bend towards the abscissa to form semicircles with their center on or below the real axis. Fig. 4.12 is further characterized by the presence of a single semi-circular arc at 308-500 K. However, in the low-frequency region, the complex impedance plot at 448-500 K, neither shows the complete semicircle nor any characteristic electrode spike rather a long residual tail exists. It may be due to the grain boundary or electrode surface effects or both depending upon the temperature. The absence of an electrode-spike indicates that the material is an electronic conductor in the non-ferroelectric orientation at 308-428 K. The semicircular arc corresponding to grain at high frequency has been suppressed due to high value of grain boundary resistance which is analogous to internal barrier layer capacitance (IBLC), characterized by semiconducting grain with insulating grain boundary. On extrapolation in the high-frequency region, the intercept on Z′ axis (in Fig 4.12), is not found to be close to zero, suggesting that there must be an existence of another semi-circle in a high-frequency region beyond the measuring frequency range. The non-zero intercept of the arc passing through the origin on Z′ axis gives the effective contribution of the grain resistance (R_g) value while that of the another arc in the lower frequency range gives contribution of grain boundaries (R_{gb}) to the total resistance.

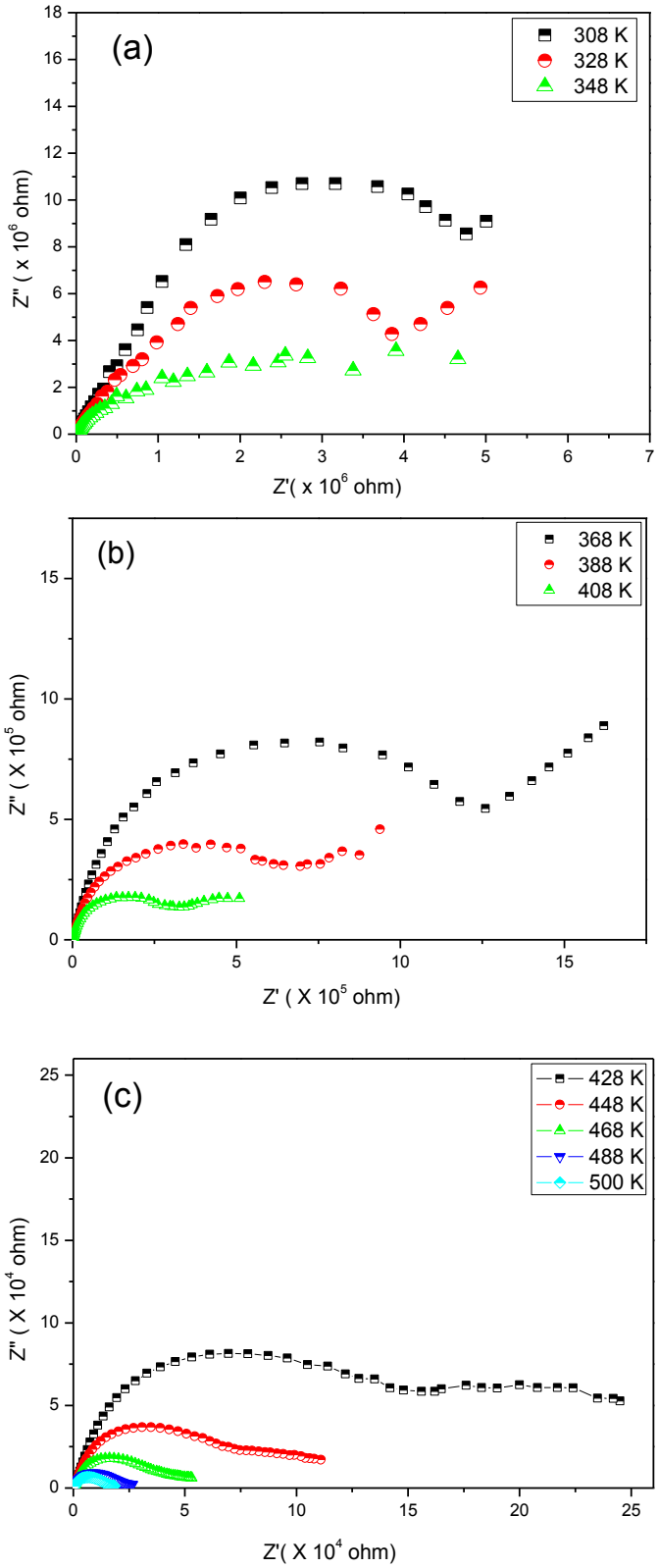

Figure 4.12: Impedance plane plots (Z′ vs Z′′) of sintered YLCTO ceramic at a few selected temperatures (a) 308-348 K (b) 368-408 K (c) 428-500 K.

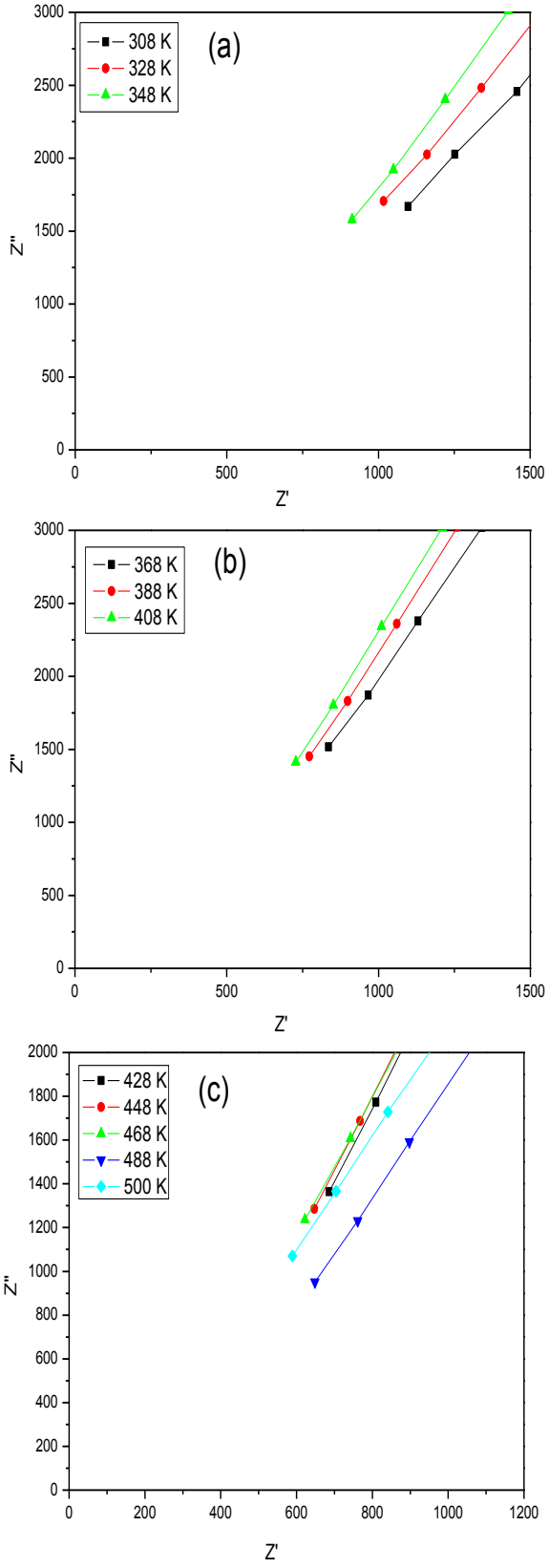

Figure 4.13: Extrapolation of Z′ vs Z″ plot in the higher frequency range at (a) 308-348 K (b) 368-408 K (c) 428-500 K to get resistance of grain for YLCTO ceramic.

The calculated values of R_g was found to be 477, 389 and 325 Ω at 308-348 K, 355, 337 and 323 Ω at 368-408 K and 323, 320, 300, 272, 253 and 247 Ω at 428-500 K which are shown in Fig, 4.13 (a), (b) and (c).

It is also observed that the radii corresponding to the size of different arcs are decreasing with increase in temperature, thereby representing the distribution of relaxation times in the YLCTO ceramic and indicating a decrease in the resistivity of the material with the increase in temperature. It is also apparent from the table that grain boundary resistance decreases with rise in temperature whereas grain resistances do not much alter with temperature confirming the semiconducting behavior of grains. From the Fig. 4.12, it can also be inferred that the resistance of grain boundary is very high in comparison to those of grains.

The variation of the imaginary part of impedance Z'' with frequency at a few selected temperatures, shown in Fig. 4.14, exhibits relaxation peaks at all measured temperatures. The decrease in magnitudes of Z'' with increase in frequency implies that relaxation in YLCTO ceramic is highly temperature-dependent and apparently there is no single relaxation time. A significant broadening of relaxation peaks with rise in temperature again confirms the existence of a temperature-dependent electrical relaxation phenomenon in the material. The asymmetric broadening of peaks in YLCTO ceramic also suggests the presence of electrical phenomena with a wide spread of relaxation time. The factors responsible for relaxation behavior in YLCTO ceramic may possibly be the presence of immobile species or electrons at a low temperature and defects or vacancies at a higher temperature. The localized relaxation in dielectric materials originating from defect relaxation dominates because of the low dielectric ratio = $\varepsilon_s/\varepsilon_\infty$, where ε_s and ε_∞ are dielectric constants at low and high frequencies, respectively. Dispersion of the resultant curves in the low frequency region at different temperatures is very clear and it appears to be merging at higher frequency, irrespective of the temperature. Such behavior is due to the presence of the space charge polarization effects at a lower frequency but at a higher frequency, it gets eliminated as reported by Dhawajam et al. (2012).

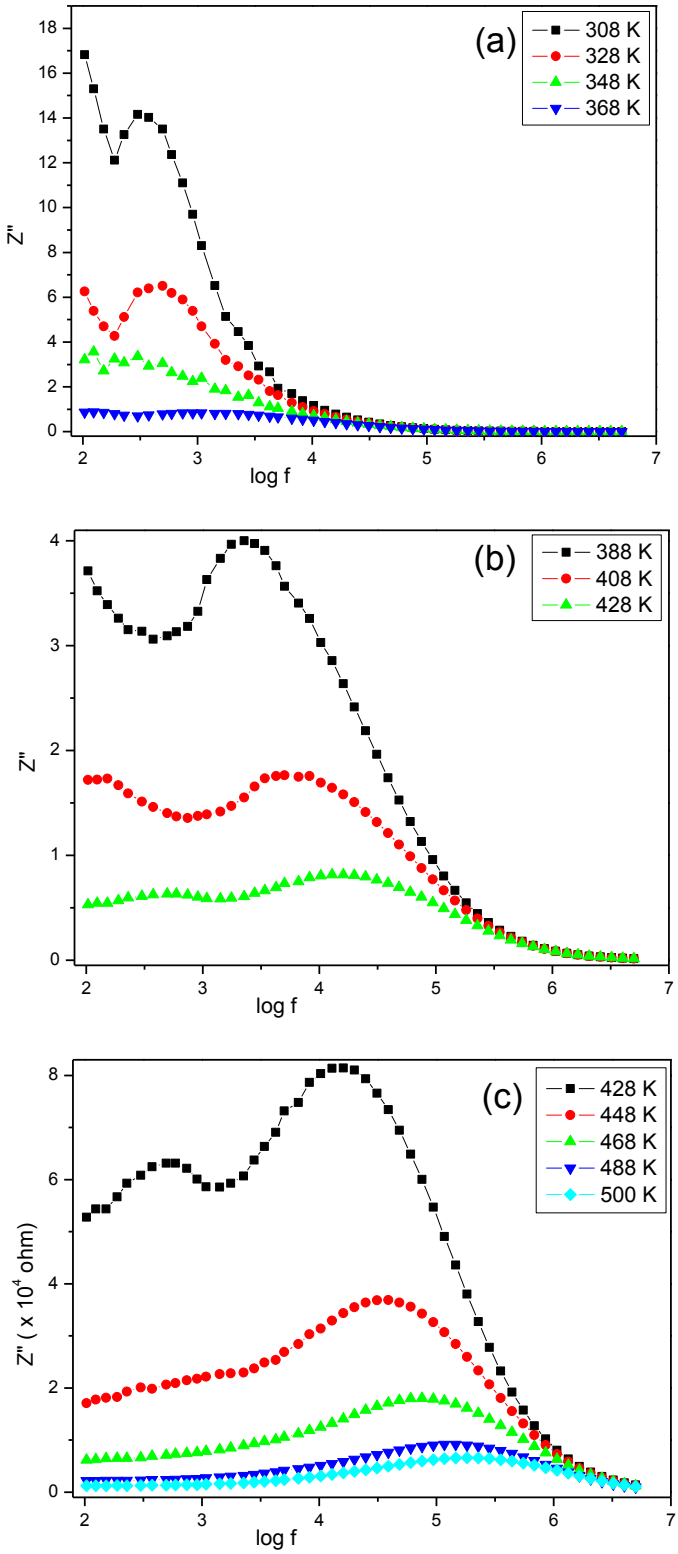

Figure 4.14: Variation of Z″ with frequency at a few selected temperatures (a) 308-348K (b) 368-408K (c) 428-500K for sintered YLCTO ceramic.

Furthermore, these peaks get suppressed and slightly shifted to a high-frequency region on increasing temperature indicating thereby the possible release of space charge accumulation at the boundaries of homogeneous phases in the test material under the applied external field. All these pieces of evidence support the existence of a temperature-dependent Maxwell-Wagner dielectric relaxation.

4.3 Conclusion

Nano-sized $Y_{1/3}La_{1/3}Cu_3Ti_4O_{12}$ ceramic was successfully synthesized by the semi-wet route using metal nitrate solution and solid TiO_2 powder in stoichiometric ratio. XRD study confirmed YCTO phase formation along with the presence of minor secondary phase of CuO. The particle size of the YLCTO ceramic was found to be 59 ± 5nm by XRD and 46 ± 8 nm by TEM studies which are in good agreement. Scanning electron micrographs shows bimodal non-uniform grain size distribution consisting of small smooth surfaced grains with some pores. Dielectric constant and loss tangent (tan δ) are temperature independent in higher frequency region but temperature dependent in low-frequency region. The impedance analysis of YLCTO ceramic shows two significant contributions associated with the grain boundaries and electrode effect. The grain-boundary resistance appears as a significant contribution at a higher temperature and electrode resistance appears at a lower temperature due to electrode polarization.